Applied Clay Science 53 (2011) 581–591

Contents lists available at ScienceDirect

Applied Clay Science

journal homepage: www.elsevier.com/locate/clay

Research Paper

Spectral characteristics of clay minerals in the 2.5–14 μm wavelength region

Fekerte Arega Yitagesu [a,b,*], Freek van der Meer [a], Harald van der Werff [a], Christoph Hecker [a]

[a] Faculty of Geo-information Science and Earth Observation, ITC of the University of Twente P.O. Box 6, 99 Hengelosestraat, 7500AA Enschede, The Netherlands
[b] The Ethiopians Road Authority, ERA P.O.Box 7129 Addis Ababa, Ethiopia

ARTICLE INFO

Article history:
Received 10 November 2010
Received in revised form 5 May 2011
Accepted 6 May 2011
Available online 8 June 2011

Keywords:
Clay minerals
Montmorillonite
Illite
Kaolinite
Spectral characteristics
PLS

ABSTRACT

Identification and quantification of clay minerals, particularly those that are responsible for susceptibility of soils to expansion and shrinkage, is a constant focus of research in geotechnical engineering. The visible, near infrared and short wave infrared wavelength regions are well explored. However, little is understood about the spectral characteristics of such clay minerals in the wavelength longer than 2.5 μm. The objective in this study was to explore the potential of laboratory spectroscopy in the 2.5–14 μm wavelength region for characterizing clay minerals. Montmorillonite, illite and kaolinite were investigated, for these clay minerals are key indicators of soil expansion and shrinkage potential. Characteristic absorption bands and their changes for mixtures of clay minerals were determined. Partial least squares (PLS) regressions in combination with continuum removal analyses were used to determine wavelength regions that best discriminate differences in mineralogical contents. Spectral contrast was high in the 3–5 μm wavelength region but overall low in the 8–14 μm. The clay minerals were characterized by strong, diagnostic absorption bands. Much of the variation in compositions of the mixtures was explained by the PLS models (coefficients of correlations of >0.90). Thus, spectroscopy in the 2.5–14 μm wavelength region is a useful technique for characterizing clay minerals.

1. Introduction

Montmorillonite, illite and kaolinite are the most common soil forming clay minerals (Fitzpatrick, 1980; Galan, 2006; Gray and Murphy, 2002). In geotechnical engineering, they are key indicators of soil expansion and shrinkage potential (Al-Rawas, 1999; Chen, 1988; Fall and Sarr, 2007; Karathanasis and Hajek, 1985; Mitchell, 1993; Seed et al., 1962; Thomas et al., 2000; Yong and Warkentin, 1975). These clay minerals are distinct in composition, structural arrangements and physicochemical characteristics (Brigatti et al., 2006; Yong and Warkentin, 1975). Montmorillonite can be formed from parent materials with high levels of calcium, ferromagnesium oxides in low content of silica under favorable environmental conditions; poorly drained environment and seasonally moderate rainfall where evaporation exceeds precipitation (Fitzpatrick, 1980; Galan, 2006; Gray and Murphy, 2002). Primary illitization can be favored by an abundance of feldspars and mica (biotite, muscovite) such as in silicic to intermediate geologic environment (Fitzpatrick, 1980; Galan, 2006), at high levels of aluminum and potassium at the expense of calcium and sodium. Illite often occurs as mixed smectite–illite interstratified minerals, exhibiting a property between the two clay minerals (Brigatti et al., 2006; Yong and Warkentin, 1975). Low concentrations of basic cations, high feldspar and silica contents, accompanied with high rainfall and temperature easing extensive leaching, favor kaolinite formation (Galan, 2006). All the three clay minerals can be found in a variety of sedimentary rocks such as mudstones, claystone and shale (Galan, 2006).

Soil expansiveness constitutes a significant challenge in geotechnical engineering (Al-Mukhtar et al., 2010; Al-Rawas, 1999; Bell, 1999; Kariuki et al., 2004; Morin and Parry, 1971; Seco et al., 2011; Shi et al., 2002; Snethen, 1975; Sridharan and Gurtug, 2004; Thomas et al., 2000). It is an intrinsic property caused by the presence of active clay minerals in soils (Fityus and Buzzi, 2009; Seed et al., 1962; Skempton, 1984; Snethen, 1975). Detection of the presence of such clay mineral is a key factor for differentiating potentially expansive soils. Identification and quantification of their abundance are essential for rating soil expansiveness. Conventional mineralogical analysis involves X-ray diffraction (XRD) analysis, scanning electron microscopy (SEM), transmission electron microscopy (TEM), differential thermal analysis (DTA), thermogravimetric analysis (TGA), and various chemical analysis methods. These methods are vital in research laboratories for exploring the basic properties of clay minerals. However, they are costly and require sophisticated laboratory procedures. Thus, they are not commonly used in soil mechanics laboratories for routine analysis of soil geotechnical characteristics. An easier alternate identification and quantification of expanding clay minerals are thus a constant focus of research in geotechnical engineering, including the application of remote sensing techniques.

Reflectance spectra of clay minerals were subjected to intensive research in the visible near infrared (VNIR) and short wave infrared (SWIR) wavelength regions (Bourguisnon et al., 2007; Chabrillat et al., 2002; Clark, 1999; Kariuki and Van der Meer, 2003; Kariuki et al., 2003; Kruse, 1991; Kruse et al., 1990; Rowan et al., 1977;

* Corresponding author at: Faculty of Geo-information Science and Earth Observation, ITC of the University of Twente P.O. Box 6, 99 Hengelosestraat, 7500AA Enschede, The Netherlands. Tel.: +31 53487416.
E-mail address: yitagesu@itc.nl (F.A. Yitagesu).

0169-1317/$ – see front matter © 2011 Elsevier B.V. All rights reserved.
doi:10.1016/j.clay.2011.05.007

Rowan et al., 2003; Van der Meer, 1995; Viscarra Rossel et al., 2009; Yitagesu et al., 2009). Particularly in the SWIR, clay minerals exhibit diagnostic absorption bands (Clark, 1999; Kariuki et al., 2004; Mustard et al., 2008; Van der Meer, 1999) resulting from vibrational processes related with their structural water molecules and hydroxyl groups (Farmer, 1974). Spectral responses of clay minerals result from vibrations of structural water molecules, hydroxyl groups, the silicate framework, and the octahedral, tetrahedral and interlayer cations (Farmer and Russell, 1964). Spectral characteristics differ, depending on the chemical composition, structural arrangement and bonding characteristics (Clark, 1999; Van der Meer, 2004) and provide a significant potential for discriminating clay minerals (Bourguisnon et al., 2007; Chabrillat et al., 2002; Frost et al., 2001; Goetz et al., 2001; Kariuki et al., 2004; Mustard et al., 2008; Roush et al., 1987; Yitagesu et al., 2009). Absorption band analysis (Clark and Roush, 1984; Goetz et al., 2001; Kariuki et al., 2003; Kariuki et al., 2004; Van der Meer, 2004) and multivariate regression analysis (Martens and Naes, 1989; Wold et al., 2001) were extensively used for estimating soil properties (Cloutis, 1996; Gomez et al., 2008; Rainey et al., 2003; Selige et al., 2006; Shepherd et al., 2005; Viscarra Rossel et al., 2006; Viscarra Rossel et al., 2009; Waiser et al., 2007), including soil geotechnical characteristics (Yitagesu et al., 2009). However, research in this respect is limited in the wavelength region longer than 2.5 μm. In this wavelength region, molecules exhibit strong, fundamental vibrations of high frequency (Arnold, 1991; Clark, 1999; Farmer and Russell, 1964; Ludwig et al., 2008). Therefore, this wavelength region is often termed a fingerprint region (Griffiths and de Haseth, 2007). The spectral sensitivity of clay minerals in this wavelength region is associated to their structural and compositional variations (Farmer and Russell, 1964). Furthermore, Famer (1974) presented infrared transmission spectra and assigned wavelengths with vibrations of clay mineral constituent molecules. Frost et al. (2001) studied absorbance spectra of sepiolites and palygorskites. They reported that the spectral changes of these minerals were related to differences in their structural arrangements and compositions. Although transmission and absorbance spectra contain similar spectral information (Michalski et al., 2006), they are not directly applicable to remote sensing, for emission or reflectance than transmittance and absorbance are detected. Roush et al. (1987) discussed reflectance spectra of kaolinite, montmorillonite and palagonite in the 2.5–4.6 μm wavelength region; and spectrally discriminated these minerals based on characteristic absorption bands at ~3 μm. Michalski et al. (2006) linked spectral emission bands of clay minerals and clay mineral bearing rocks to crystal chemical properties. They also reported detection of poorly crystalline clay minerals in the 6–25 μm wavelength region with the thermal emission spectrometer (TES) on Mars that were previously not easily detectable in the VNIR and SWIR wavelength regions. Other researchers (Cooper and Mustard, 1999; Hecker et al., 2010; Johnson et al., 1998; Salisbury and D'Aria, 1992, 1994; Salisbury et al., 1994) demonstrated the spectral behavior of different minerals and discussed various issues related with spectral data acquisitions and interpretations. Among the clay science society, there is a growing interest in Fourier transform infrared (FTIR) spectroscopy, as it allows a rapid, economical and nondestructive method for investigating clay minerals (Petit, 2006).

The objectives in this study were to explore the potential of laboratory spectroscopy in the 2.5–14 μm wavelength region for detection, identification and quantification of clay minerals, thereby determining characteristic absorption bands and their variation in clay mineral mixtures. Experimental investigations were carried out with the three clay minerals that were established to be vital with respect to soil expansiveness. This study on pure clay minerals, and known mixtures of these clay minerals, aimed at an understanding of the manifestations of such clay minerals in natural soils. Emphasis was given to the 3–5 μm and 8–14 μm wavelength regions, to provide an outlook for a remote sensing implication.

2. Materials and methods

2.1. Sample preparation

Experiments were conducted on pure clay minerals: montmorillonite, illite, kaolinite and their proportioned mixtures. The clay mineral specimens were commercially supplied by VWR international (https://www.vwrsp.com), as powders (particle size <2 μm). Mixtures were prepared at 20% by mass increments composing totals of 100 g. The specimens were weighted on a top loading precision balance (of ±1 g precision, model: Mattler PE 360), then poured into a porcelain mortar bowl and stirred by a spatula for about five minutes to get homogenous mixtures. Spectral measurements were done on loosely packed, randomly oriented specimens. The spectra were acquired in the 2.5–14 μm wavelength region, using a Bruker Vertex 70 Fourier transform infrared spectrometer (http://www.brukeroptics.com). The spectrometer was equipped with an accessory mode integrating sphere, coated inside with a diffusely reflecting gold surface, which was attached to its external port. This enabled directional hemispherical spectral reflectance measurements. With such a setup, Kirchhoff's law can be used to derive the directional spectral emissivity (Johnson et al., 1998; Salisbury and D'Aria, 1994). The spectrometer was configured to provide spectral reflectance with 4 cm^{-1} spectral resolution at 512 scans per each measurement and eight measurements per specimen, which were later averaged for a better signal to noise ratio. Referencing was done before each sample measurement against a gold-coated plate having the same surface as the inside wall of the integrating sphere. The spectrometer was continuously purged with nitrogen gas, to remove any water vapor and carbon dioxide from the system. Liquid nitrogen was used for cooling the detector. The OPUS spectroscopy software version 6.5 (Bruker Optik GmbH, 2007) in a desktop system which is integrated with the spectrometer was used for parameter setting and visualization of the acquired spectra.

2.2. Spectral analysis

Two approaches were followed. The first was an evaluation of the shape and intensity of the spectra, absorption bands and their changes such as the depth, position, width and area (Gaffey, 1986; Van der Meer, 1995, 2004) relative to compositions of the mixtures. Second, a quantitative estimation of the compositions of mixtures from the spectra using a multivariate calibration technique, partial least squares regression analysis (Shepherd et al., 2005; Viscarra Rossel et al., 2006; Waiser et al., 2007; Yitagesu et al., 2009). The multivariate quantitative analyses were limited to the 3–5 μm and 8–14 μm wavelength region. The analyses were conducted on continuum removed spectra. A continuum is a mathematical function used to isolate specific absorption bands (Clark and Roush, 1984). It corresponds to the background or overall albedo of the reflectance curve (Van der Meer, 2004). The continuum can be calculated using straight lines, Gaussians and modified Gaussians, polynomials and splines (Clark and Roush, 1984; Fu et al., 2007; Sunshine et al., 1990; Van der Meer, 2004). A classical continuum removal modeled by straight line segments tangential to the spectra (Clark and Roush, 1984; Clark et al., 1987; Van der Meer, 2004) built in the ENVI software (ITT Visual Information Solutions, 2009) was used. ENVI uses an automated algorithm described by Clark et al. (1987) to find maximum tie points for fitting straight line segments and establish the continuum line, then remove the continuum by dividing it into the original spectrum. Van der Meer (2004) reported that continuum removal enhances all absorption bands including noise. Hence, careful selection of wavelength regions is essential. The continuum removal was done independently for the 3–5 μm and 8–14 μm wavelength regions, due to differences in spectral contrast.

2.3. Partial least squares regression analysis

Partial least squares (PLS) regression analysis is a fundamental statistical tool for estimating soil properties from reflectance spectra (Cloutis, 1996; Rainey et al., 2003; Shepherd et al., 2005; Viscarra Rossel et al., 2006; Waiser et al., 2007; Yitagesu et al., 2009). PLS1 (Martens and Naes, 1989), built in The Unscrambler software (CAMO Process AS, 2005) was used to establish relationships among the spectra and clay mineral contents. The 3–5 μm and 8–14 μm wavelength regions were analyzed separately. Before the PLS regression analyses, the distributions of variables were checked, and appropriate transformations were carried out on variables that showed skewed distribution. As described by Martens and Naes (1989) and Wold et al. (2001), the data were mean centered and scaled to unit variance before calibration, for enhancing variance in the explanatory data and removing any systematic bias. A full cross validation method based on a leave one out principle was used to calibrate and validate the prediction models. PLS component selections were based on evaluation of residual and explained variances, and corresponding root mean square errors. Thus, factors with low residual variances accompanied with low root mean square errors were selected. The model performance was assessed by various statistics and graphical outputs, as outlined by Martens and Naes (1989). Coefficients of correlations (R) and coefficients of determinations (R^2) served to

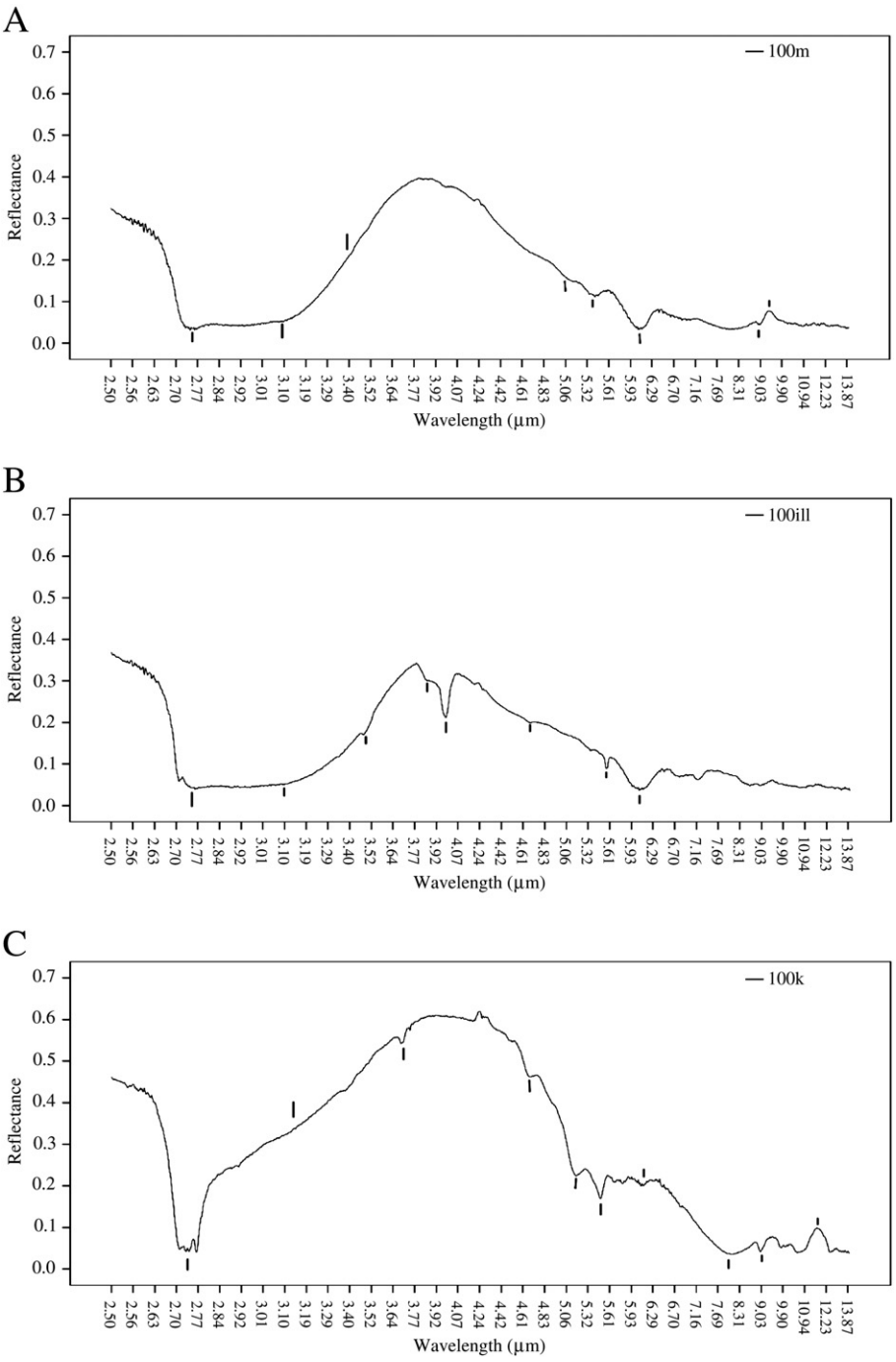

Fig. 1. Spectra of (A) montmorillonite, (B) illite, and (C) kaolinite in the 2.5–14 μm wavelength region, with spectral characteristics annotated with lines.

evaluate the goodness of fits. Expected prediction errors were assessed using the root mean square errors of predictions (RMSEP). Standard errors of performance (SEP), which were computed as the standard deviation of the residuals indicated the precision of the predictions over the whole samples. Bias showed interference errors and was computed as an average value of the variations that were not taken into account by the models. Offset showed the point where regression lines crossed the ordinate in the scatter plots, summarizing the relationship between measured and predicted values of the response variables, thus showed possible deviations from ideal one to one correspondences. Graphical outputs such as score plots, stability plots, scatter plots of X–Y relation outliers, and scatter plots of the measured versus predicted responses were also examined. These graphs were used to check sample distributions, identify samples causing perturbation, detect outliers and assess the nature of relationships among the predictors and responses such as deviation from linearity, and the quality of the regression models in terms of fitting the data respectively. Plots of B-coefficients were used to visualize significant wavelengths for predicting clay mineral contents. These coefficients were used to build model equations. Weighted coefficients B_{ow} and raw coefficients B were identical, because no weighting was applied on the variables.

3. Results

3.1. Spectral characteristics of the clay minerals

3.1.1. Montmorillonite, illite, kaolinite

The spectra of montmorillonite (Fig. 1A), illite (Fig. 1B), and kaolinite (Fig. 1C) were well resolved in the 2.5–14 μm wavelength region. All spectra exhibited strong, broad absorption bands in the 2.5–3.7 μm wavelength region, with absorption minima at ~2.75 μm and ~3.1 μm for montmorillonite and illite, being generally broader in the illite spectrum. The kaolinite spectrum showed asymmetric and sharply defined absorption minimum centered at ~2.75 μm.

The montmorillonite spectrum was further characterized by rounded troughs at ~5.1 μm and ~5.4 μm. The prominent absorption band centered at ~6.1 μm, according to Farmer (1974) is typical of water bearing clay minerals and is associated with the bending vibrations of structural water molecules (Frost et al., 2001). Near 9.4 μm, montmorillonite exhibited reflectance maxima following an absorption deep at ~9 μm.

In the illite spectrum, weak troughs were seen at ~3.48 μm and ~4.67 μm. The doublet with absorption minima at ~3.84 μm and ~3.98 μm was intense and sharp at the later. The narrow, intense absorption band at ~5.56 μm was followed by a broader absorption band at ~6.1 μm.

A slight minimum at ~3.69 μm and a doublet at ~5.2 μm and ~5.5 μm seemed to be diagnostic of kaolinite. In addition, the kaolinite spectrum showed weak troughs at ~4.7 μm, ~8.6 μm, ~9.8 μm, ~10.6 μm and ~12.4 μm; and reflectance peaks at ~6.3 μm, ~9.4 μm and ~11.7 μm.

3.1.2. Mixtures of montmorillonite and kaolinite

Overall line shapes and reflectance intensities of the spectra of montmorillonite, kaolinite and their mixtures exhibited characteristic differences (Fig. 2). The absorption bands at 2.5–3.7 μm varied with the montmorillonite/kaolinite ratio. The sharp, asymmetric absorption minimum at ~2.75 μm in kaolinite became poorly defined with increasing montmorillonite content. The absorption minimum at ~3.1 μm, which is typical of water bearing clay minerals (Farmer and Russell, 1964; Roush et al., 1987), subtly shifted to lower wavelengths as the kaolinite content increased. The weak trough at ~3.69 μm in kaolinite gradually disappeared with increasing montmorillonite content. The slopes of the spectra in the ~3–3.5 μm increased with the kaolinite content. The continuum removal enhanced the changes in absorption bands in the 3–5 μm (Fig. 3A) and 8–14 μm (Fig. 3B) wavelength regions. The changes seemed to correspond to the montmorillonite/kaolinite ratio. While the depth of the band centered at ~3.1 μm increased with increasing montmorillonite content, its position shifted to longer wavelengths. Similarly, the depth of the water molecule absorption band at ~6.1 μm increased with increasing montmorillonite content. In a 100% kaolinite spectrum, the ~6.1 μm absorption band entirely disappeared. Its position slightly shifted towards longer wavelengths with increasing kaolinite content (Fig. 3C). The doublet with minima at ~5.2 μm and ~5.5 μm in kaolinite became rounded and less pronounced with increasing montmorillonite content; and disappeared at <40% kaolinite. The rounded troughs in montmorillonite at ~5.1 μm and ~5.4 μm, subtly disappeared in the spectra of samples at high kaolinite contents. Additionally, the sharp absorption band at ~9 μm slightly varied in depth, and the ~11.6 μm reflectance intensity increased with increasing kaolinite content.

3.1.3. Mixtures of illite and kaolinite

The spectra of illite, kaolinite and their mixtures differed in overall shapes and reflectance intensities (Fig. 4). The absorption bands at 2.5–3.7 μm varied with changes in the mineralogical compositions.

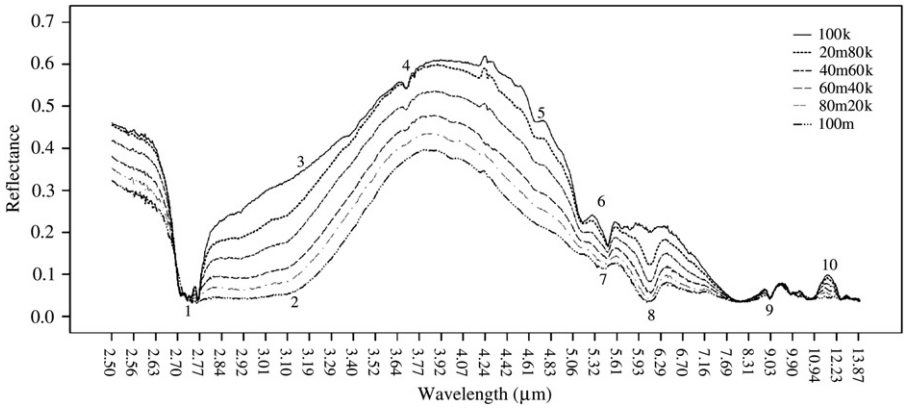

Fig. 2. Spectra of montmorillonite, kaolinite and their mixtures, annotated with numbers, showing changes in characteristic bands. (1) Changes in absorption minima at ~2.75 μm with changing montmorillonite/kaolinite ratio. (2) Shifts in position at ~3.1 μm. (3) Slope differences at 3–3.5 μm. (4) Variations in the absorption band at ~3.7 μm, (5) modest band at ~4.7 μm, and (6) doublet with minima at ~5.2 μm and ~5.5 μm for kaolinite. (7) Changes in the rounded troughs at ~5.1 μm and ~5.4 μm for montmorillonite. (8) Changes in intensity of absorption bands at ~6.1 μm, and (9) ~9 μm with changing montmorillonite/kaolinite ratio. (10) Differences in reflectance intensity at ~11.6 μm with increasing kaolinite content. (k = kaolinite and m = montmorillonite with prefix numbers showing contents in percent.).

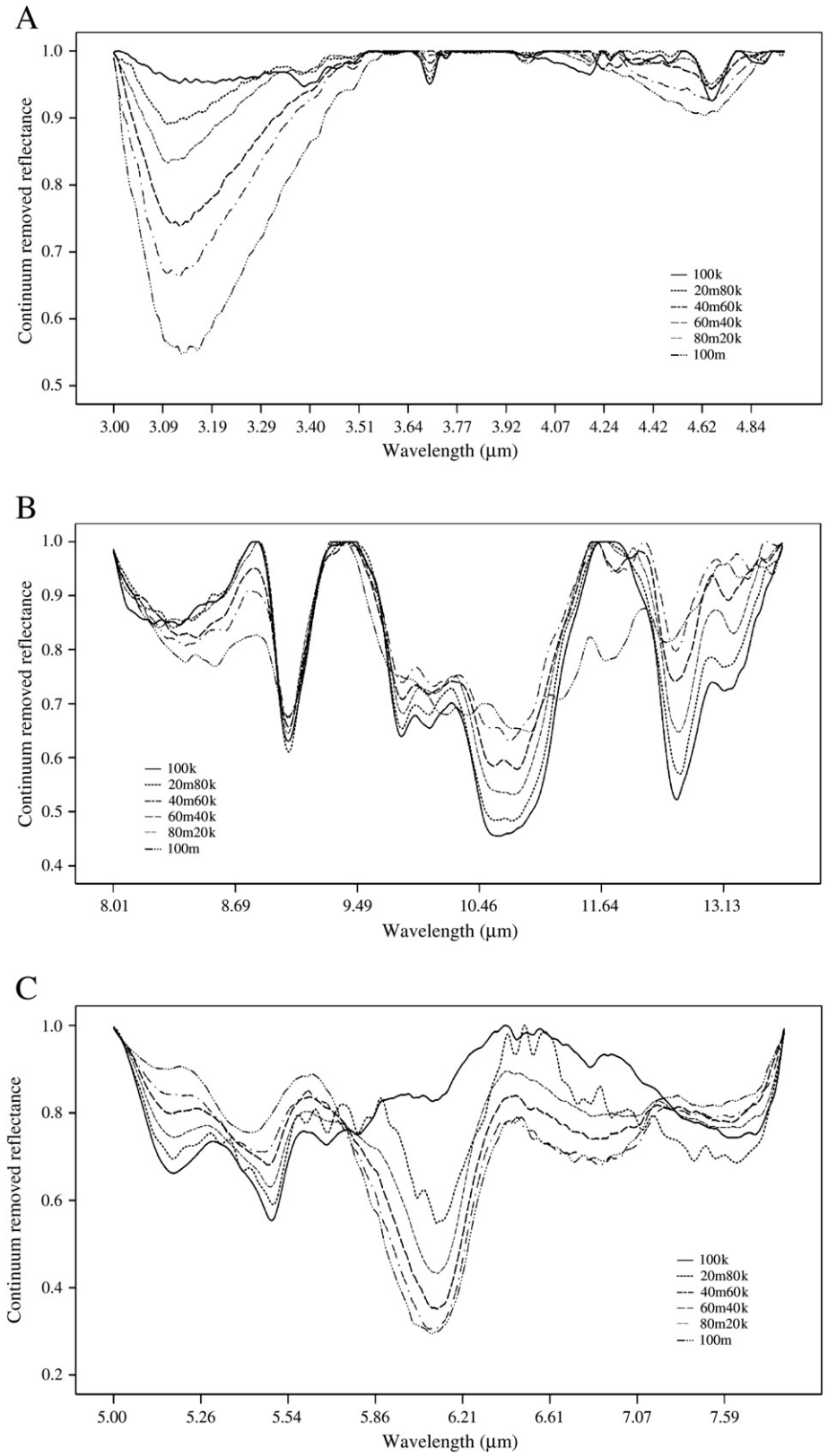

Fig. 3. Continuum removed spectra of montmorillonite, kaolinite and their mixtures, showing variations corresponding to changes in mineral contents: at the (A) 3–5 μm, (B) 8–14 μm and (C) 5–8 μm wavelength regions. Note the changes at the band centered (A) ~3.1 μm, (B) ~8.5 μm, ~10.6 μm, and ~12.4 μm to ~13.5 μm, (C) ~6.1 μm, and the intensity of the doublet at ~5.2 μm and ~5.5 μm for kaolinite. (k = kaolinite and m = montmorillonite with prefix numbers showing contents in percent.).

The sharp absorption minimum at ~2.75 μm became poorly defined with increasing illite content. The slopes of the spectra at ~3–3.5 μm progressively increased with increasing kaolinite content. The continuum removal of the spectra in the 3–5 μm wavelength region (Fig. 5A) enhanced differences in depth and position of the band at ~3.1 μm. While the depth increased with increasing illite content, its

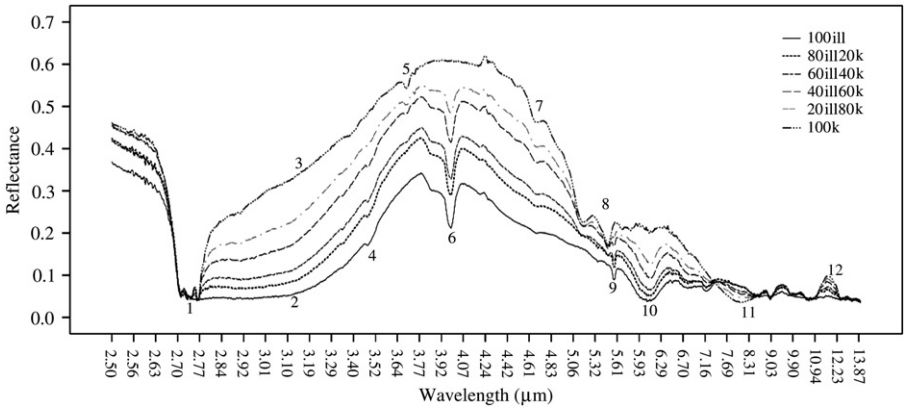

Fig. 4. Spectra of illite, kaolinite and their mixtures, annotated with numbers, showing characteristic spectral differences. (1) Changes in absorption minima at ~2.75 μm. (2) Shifts in positions at ~3.1 μm. (3) Slope differences at 3–3.5 μm. (4) The weak trough at ~3.48 μm for illite that disappeared in the spectra of samples with high kaolinite content. (5) The modest absorption band at ~3.69 μm for kaolinite that disappeared in the spectra of samples at <80% kaolinite. (6) Changes in intensity of the doublet at ~3.84 μm and ~3.98 μm for illite. (7) The weak trough at ~4.7 μm for kaolinite that disappeared as illite content increased. (8) The doublet for kaolinite that gradually disappeared in the spectra of samples with high illite content. (9) Changes in the intensity of the narrow absorption band at ~5.56 μm for illite. (10) Changes in intensity of the band at ~6.1 μm. (11) Variations in reflectance intensity at ~8.10 μm, and (12) ~11.6 μm, with changing illite/kaolinite ratio. (k = kaolinite and ill = illite with prefix numbers showing contents in percent.).

position shifted to longer wavelengths. The weak trough at ~3.48 μm for illite disappeared with increasing kaolinite content. The modest deep in the kaolinite spectrum at ~3.69 μm disappeared at <80% kaolinite. The depth of the doublet at ~3.84 μm and ~3.98 μm in the illite containing samples spectra lowered with increasing kaolinite content. The intensity of the narrow absorption band at ~5.56 μm for illite also decreased with decreasing illite content. The doublet band in the kaolinite spectrum gradually disappeared with increasing illite content and was absent at illite content >60%. The water molecule absorption band at ~6.1 μm decreased with increasing kaolinite content (Fig. 5C). This decrease in intensity was accompanied with a shift of the position towards longer wavelengths.

3.1.4. Mixtures of montmorillonite and illite

The spectra of montmorillonite and illite overlapped at the water absorption bands centered at ~3.1 μm and ~6.1 μm. The positions of these absorption bands subtly varied with changing montmorillonite/illite ratio. Both bands became broad with increasing illite content (Figs. 6 and 7A). The spectra of montmorillonite containing samples showed rounded troughs at ~5.1 μm and ~5.4 μm. The spectra of illite containing samples showed modest deeps at ~3.48 μm, doublets with absorption minima at ~3.84 μm and ~3.98 μm, and narrow, intense absorption bands at ~5.56 μm. The intensity of the doublets with absorption minima at ~3.84 μm and ~3.98 μm, and the narrow absorption bands at ~5.56 μm decreased with decreasing illite content. Both bands appeared in the presence of illite. Therefore, these bands were the prominent bands for differentiating illite and montmorillonite.

3.2. Estimation of clay mineral contents

Pair-wise correlation analyses showed that the mean reflectance in the 2.5–14 μm wavelength region were strongly correlated with the clay mineral compositions at 0.01 significance levels. The clay mineral compositions in montmorillonite–kaolinite, illite–kaolinite, and montmorillonite–illite mixtures were negatively related to the mean reflectance at Pearson correlations of −0.99, −0.98 and −0.90, respectively. These correlations indicated that absorption bands and clay mineral compositions are linearly related. The correlation in the montmorillonite–illite mixtures was lower than for montmorillonite–kaolinite and illite–kaolinite mixtures. This is probably due to the similar structure of the two water bearing clay minerals, which might in turn, determine their spectral characteristics.

Significant wavelengths for estimating the contents of montmorillonite and illite from the spectra of montmorillonite–kaolinite (Fig. 8A and B), illite–kaolinite (Fig. 8C and D), and montmorillonite–illite (Fig. 8E and F) mixtures are presented for the 3–5 μm and 8–14 μm wavelength regions. Table 1 shows; the correlation coefficients, root mean square error of the predictions, standard error of performances, biases and offsets. Much of the variation in the clay mineral compositions was explained by the PLS models. A better agreement was achieved at 3–5 μm wavelength region than at 8–14 μm. The relation was again weaker, particularly for the montmorillonite–illite mixtures, where the coefficient of correlation was lower, and the model error terms were higher (Table 1) than those obtained for montmorillonite–kaolinite and illite–kaolinite mixtures.

4. Discussion

Montmorillonite, illite, kaolinite, and their mixtures showed spectrally distinct bands. The overall shape and intensity of the bands varied with the clay mineral contents. Thus, as described by Clark and Roush (1984), Gaffey (1986) and Van der Meer (1995 and 2004) these spectral changes were effective measures of compositions of the mixtures. The strong absorption band in the 2.5–3.7 μm wavelength region, in the spectrum of montmorillonite (Fig. 1A), exhibited minima at ~2.75 μm and ~3.1 μm. Hunt (1977) assigned the band at ~2.75 μm to fundamental vibrations of hydroxyl groups, at ~2.9 μm to asymmetric stretching of hydroxyl groups, at ~3 μm to overtone bending vibrations of water molecules, and the band at ~3.1 μm to asymmetric stretching vibration of H–O of the water molecules. The overlapping vibrations of structural hydroxyl groups and water molecules (Farmer, 1974) broadened absorption bands in the illite spectrum (Fig. 1B). In kaolinite, the asymmetric stretching of hydroxyl groups (Farmer, 1974; Farmer and Russell, 1964) produced a deep and narrow absorption band centered at ~2.75 μm (Fig. 1C). Changes took place when montmorillonite and kaolinite were heated (Roush et al., 1987). The ~2.75 μm band became narrower in montmorillonite due to the loss of water molecules. Little changes occurred in kaolinite spectrum due to the absence of water molecules. The wide absorption band exhibited in the illite spectrum can be associated with the substitution of Al for Si (Yong and Warkentin, 1975). The bands at ~3.1 μm and ~6.1 μm were prominent in the spectra of montmorillonite and illite containing samples (Figs. 2, 3A,C, 4, 5A,C, 6, and 7A), due to the similar structure of these clay minerals (Brigatti et al., 2006). The band intensity decreased with increasing

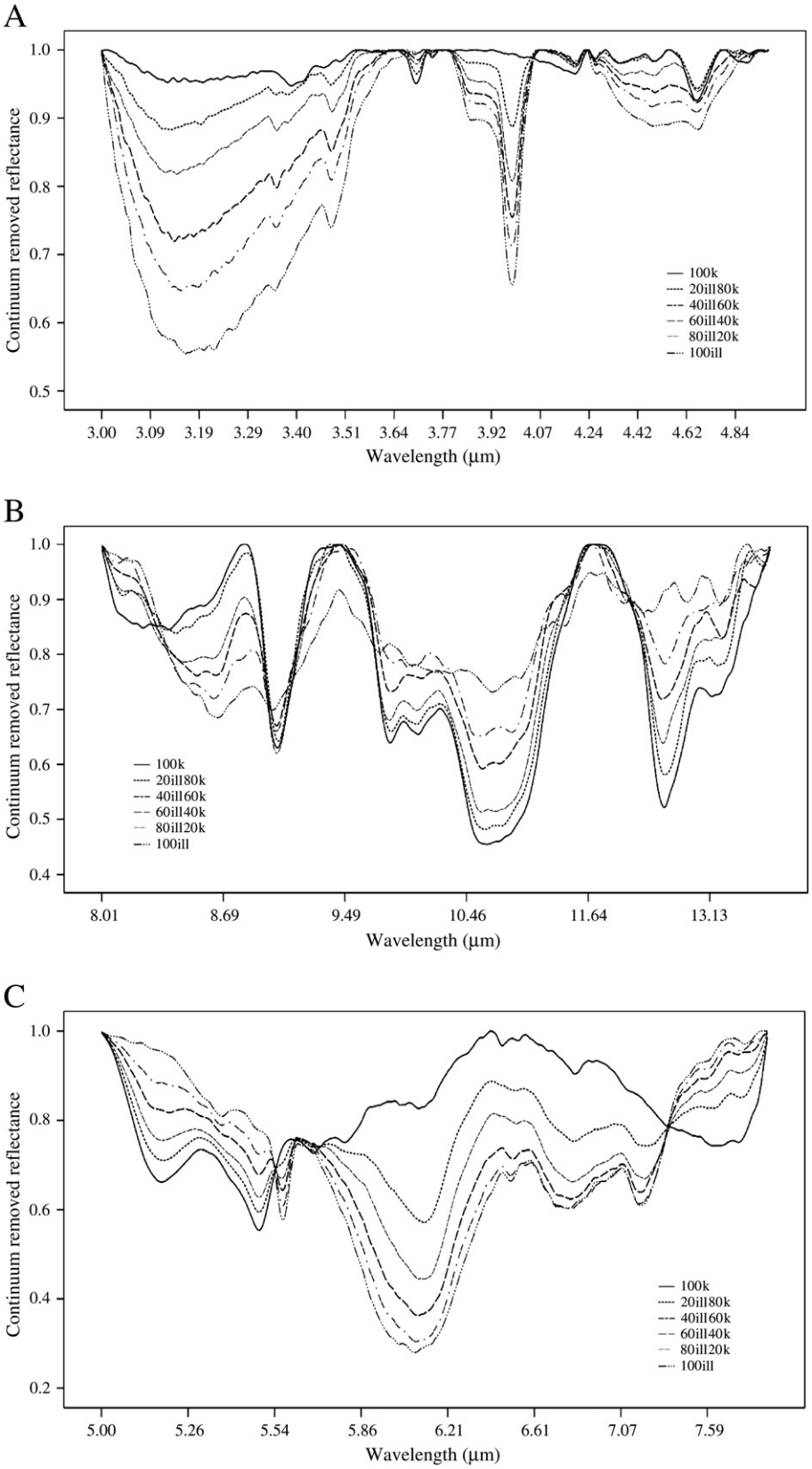

Fig. 5. Continuum removed spectra of illite, kaolinite, and their mixtures showing variations of bands corresponding to changes in compositions of the mixtures: in the (A) 3–5 μm, (B) 8–14 μm and (C) 5–8 μm wavelength region. Note the changes at the band centered (A) ~3.1 μm, (B) ~8.5 μm, 10.6 μm, ~12.4 μm to ~13.5 μm, and (C) ~6.1 μm. The doublet for kaolinite became rounded at high illite contents. The narrow, intense absorption band at ~5.56 μm for illite subtly decreased as kaolinite content increased. (k = kaolinite and ill = illite with prefix numbers showing contents in percent.).

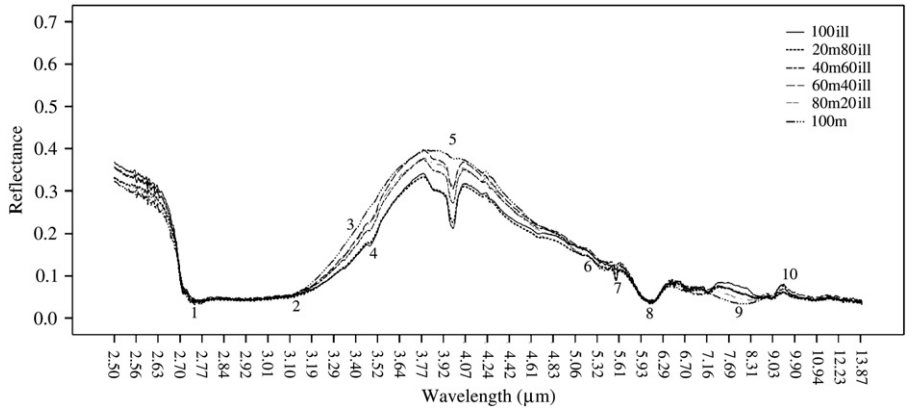

Fig. 6. Spectra of illite, montmorillonite, and their mixtures, annotated with numbers, showing characteristic spectral differences with changing montmorillonite/illite ratio. (1) Changes in absorption minima at ~2.75 μm. (2) Subtle shifts in positions to longer wavelengths of the ~3.1 μm with increasing illite content. (3) Slope differences at 3–3.5 μm. (4) Variations in the weak trough at ~3.48 μm for illite. (5) Variations in intensity of the doublet at ~3.84 μm and ~3.98 μm for illite. (6) Changes in the rounded troughs for montmorillonite at ~5.1 μm and ~5.4 μm. (7) Changes in the narrow, intense band at ~5.56 μm with decreasing illite content. (8) Faint variations in position and intensity of the band at ~6.1 μm. (9) Variations in reflectance intensity at ~8.10 μm, and (10) at ~9.4 μm with changing montmorillonite/illite ratio. (m = montmorillonite and ill = illite with prefix numbers showing contents in percent.).

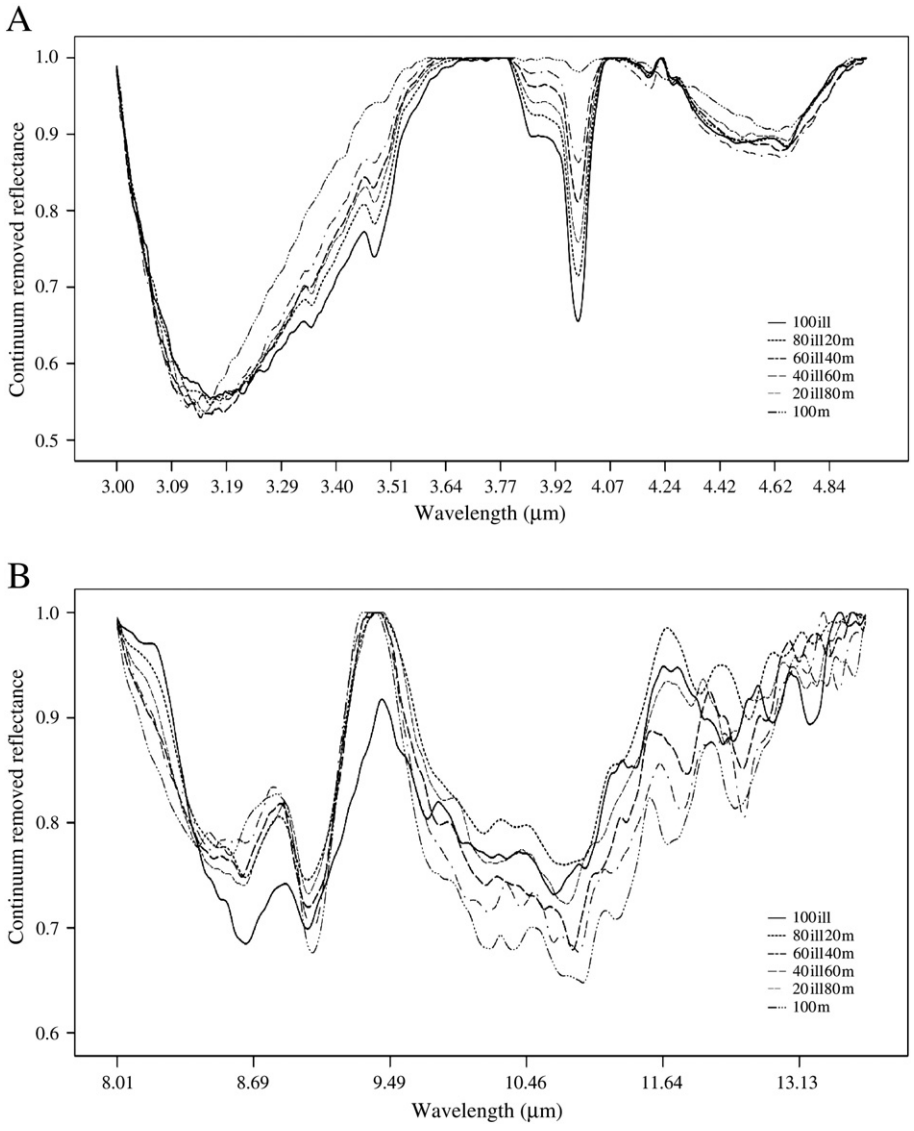

Fig. 7. Continuum removed spectra of montmorillonite, illite and their mixtures, showing changes in spectral characteristics: in the (A) 3–5 μm and (B) 8–14 μm wavelength region. The intensity of the water absorption band at ~3.1 μm increased subtly accompanied with slight shifts of positions to shorter wavelengths as montmorillonite content increased. Conversely, as the illite content increased the intensity of this band slightly decreased associated with shifts in positions towards longer wavelengths. (m = montmorillonite and ill = illite with prefix numbers showing contents in percent.).

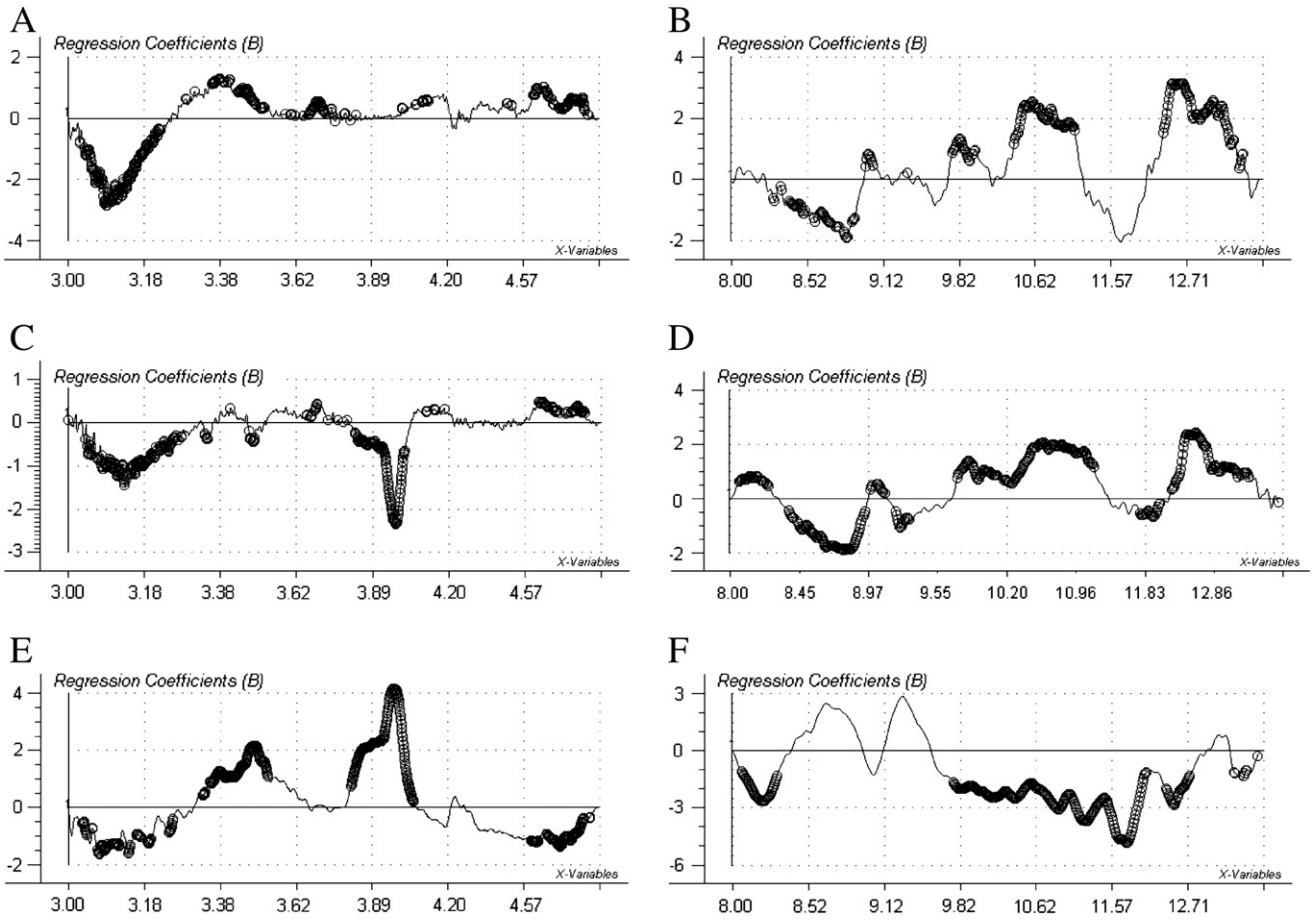

Fig. 8. PLS analyses results for estimating the clay mineral contents from spectra of montmorillonite–kaolinite mixtures in the wavelength region (A) 3–5 μm and (B) 8–14 μm; illite–kaolinite mixtures in the wavelength region (C) 3–5 μm and (D) 8–14 μm; montmorillonite–illite mixtures in the wavelength region (E) 3–5 μm and (F) 8–14 μm. Statistically significant regression coefficients (wavelengths) are highlighted in black circles.

kaolinite contents in montmorillonite–kaolinite (Fig. 3A and C) and illite–kaolinite (Fig. 5A and C) mixtures. This strong, negative relationship between the kaolinite content and intensity of these absorption bands is attributed to lack of water molecules in kaolinite. In the PLS models, the significant, opposite contributions of the wavelengths between 3 and 3.2 μm in the montmorillonite–kaolinite (Fig. 8A), montmorillonite–illite (8E) and illite–kaolinite (Fig. 8C) mixtures were similarly attributed to differences in the structure and water molecules. Concerning the structural hydroxyl groups coordinated to the octahedral cations (Brigatti et al., 2006; Gillot, 1987), substitution of cations can shift the positions of the absorption bands (Farmer, 1974). This probably explains the shifts in positions of absorption bands in the clay mineral mixtures as suggested by van der Meer (1995) as shifts in positions are characteristics of cation substitutions. Therefore, shifts in the band positions, in the spectra of montmorillonite–illite mixtures (Figs. 6 and 7A) are probably related with reorientation of the hydroxyl groups, due to substitution of Fe and Mg for Al, or Al for Si (Farmer and Russell, 1964; Yong and Warkentin, 1975). The broad absorption band centered at ~3.1 μm in the spectra of samples with illite might be further associated with distortion in the structure to accommodate longer bonds resulting from replacement of Al for Si (Farmer and Russell, 1964; Yong and Warkentin, 1975). Illite exhibited distinct doublet bands at ~3.84 μm and ~3.98 μm. The unique presence of this doublet in all spectra of illite containing samples (Figs. 4, 5A, 6 and 7A) and the narrow, intense absorption band at ~5.56 μm, which also appeared in the presence of illite can be considered diagnostic bands. These bands and the weak absorption at ~3.48 μm were significant PLS regression coefficients in estimating illite contents from mixtures of illite–kaolinite (Fig. 8C) and illite–montmorillonite (Fig. 8E).

As established by many experts, the 8–14 μm wavelength region is dominated by absorption bands resulting from SiO, hydroxyl and metal–hydroxyl vibrations (Clark, 1999; Farmer and Russell, 1964; Frost et al., 2001; Michalski et al., 2006). Michalski et al. (2006) reported that clay minerals exhibited absorption bands centered in the 9–10 μm wavelength region, due to the SiO stretching vibration. They assigned absorption bands in the 10–14 μm wavelength region to metal–hydroxyl bending vibrations. Frost et al. (2001) associated the bands at ~8–10 μm wavelength region with the SiO stretching and those at ~10–14 μm with hydroxyl groups bending vibrations. Farmer and Russell (1964) similarly assigned wavelength regions of 8–10 μm to (Al, Si)-O stretching vibrations in the tetrahedral sheets, and those of 10–14 μm to the hydroxyl and metal–hydroxyl bending vibrations

Table 1
Summary of the models performance, showing correlation coefficients in the 3–5 μm and 8–14 μm wavelength regions with corresponding RMSEP, SEP, Bias and offsets. Better agreement was achieved at 3–5 μm wavelength region.

Spectral region	Clay mineral mixtures	Correlation coefficient	RMSEP	SEP	Bias	Offset
3–5 μm	Montmorillonite–kaolinite	0.99	3.46	3.79	-0.12	2.96
8–14 μm	Montmorillonite–kaolinite	0.96	10.86	11.56	-2.58	9.07
3–5 μm	Illite–kaolinite	0.99	2.11	2.29	0.26	-0.46
8–14 μm	Illite–kaolinite	0.99	4.08	4.46	-0.34	3.78
3–5 μm	Montmorillonite–illite	0.99	2.87	3.13	-0.28	-0.37
8–14 μm	Montmorillonite–illite	0.90	15.33	16.33	3.61	15.05

in the octahedral sheets. The spectra of the clay minerals investigated here showed a sharp absorption band near 9 μm, which is probably due to the SiO stretching vibration. However, this band seems to be not a diagnostic band because it showed overlapping bands of kaolinite and montmorillonite, while it appeared shallower, with its shoulder shifted to the longer wavelength in the illite spectrum. The appearance of this band in illite might also be influenced by distortion in structure caused by substitution of Al for Si, shifts the positions to longer wavelengths (Farmer and Russell, 1964; Michalski et al., 2006). Other bands centered at ~8.6 μm, ~10.6 μm and ~12.4 μm showed significant variations that seemed to correspond to changes in the mineralogical composition (Figs. 3B, 5B and 7B). Thus, they were useful in discriminating the clay minerals as well as in estimating content of the clay minerals in the mixtures (Fig. 8B,D and F). The bands at ~10.6 μm and ~12.4 μm appeared strong and well structured in the presence of kaolinite (Figs. 3B and 5B) probably due to higher contents of aluminum relative to the other cations in the octahedral sites (Brigatti et al., 2006; Farmer and Russell, 1964). Overall, the spectral variation in the clay mineral mixtures was largely due to mineralogical variation. The absorption bands were strong and enabled a clear differentiation of the clay minerals. The presented data are seen useful to estimate the clay mineral contents in expansive soils, and thereby making rational spectral–compositional correlations.

5. Conclusions

Spectroscopy in the 2.5–14 μm wavelength region was explored for clay mineralogical characterization. The clay minerals and mixtures exhibited distinct spectral characteristics. Spectral shape, reflectance, absorption bands, and spectral contrast differed in the 3–5 μm and 8–14 μm wavelength regions. The PLS models explained much of the variations in the clay mineral compositions. Significant bands that appeared diagnostic in differentiating the clay minerals were identified. For all mixtures, the 3–5 μm wavelength region was more suited than the 8–14 μm wavelength region. The 5–8 μm wavelength region also provided valuable spectral differences among the clay minerals and mixtures. The approach demonstrated that spectroscopy in the 2.5–14 μm wavelength region is a useful technique for characterizing (detecting, identifying and quantifying) clay minerals.

Acknowledgments

The authors would like to express their deepest gratitude to Drs. Boudewijn de Smeth, of the University of Twente, Faculty of Geo-information Science and Earth Observation (ITC), who kindly facilitated the provision of clay minerals from VWR international. Mr. Henk Wilbrink is also acknowledged for providing assistance during the laboratory work. Comments from the anonymous reviewers and the editor have substantially improved the manuscript.

References

Al-Mukhtar, M., Lasledj, A., Alcover, J.-F., 2010. Behavior and mineralogy changes in lime-treated expansive soil at 20 °C. Applied clay science 50, 191–198.
Al-Rawas, A.A., 1999. The factors controlling the expansive nature of the soils and rocks of northern Oman. Engineering Geology 53, 327–350.
Arnold, G., 1991. Measurements of the spectral emittance of particulate minerals and some remote-sensing implications. Vibrational Spectroscopy 2, 245–249.
Bell, F.G., 1999. Geological hazards: their assessment, avoidance and mitigation: London etc. E & FN SPON. 648 p.
Bourguisnon, A., Delpont, G., Chevrel, A., Chabrillat, S., 2007. Detection and mapping of Shrink–Swell clays in SW France, using ASTER imagery. Geological society of London, London. 117–124 p.
Brigatti, M.F., Galan, E., Theng, B.K.G., 2006. Structures and mineralogy of clay minerals. In: Bergaya, F., Theng, B.K.G., Lagaly, G. (Eds.), Handbook of Clay Science: Developments in Clay Science, Volume 1. Elsevier, Amsterdam.
Bruker Optik GmbH, 2007. OPUS Version 6.5: Germany. http://www.brukeroptics.com 2007.
CAMO Process AS, 2005. The Unscrambler Version 9.2. CAMO, Oslo.
Chabrillat, S., Goetz, A.F.H., Krosley, L., Olson, H.W., 2002. Use of hyperspectral images in the identification and mapping of expansive clay soils and the role of spatial resolution. Remote Sensing of Environment 82, 431–445.
Chen, F.H., 1988. Foundation on Expansive Soils. Elsevier Science Publishers.
Clark, R.N., 1999. Spectroscopy of rocks and minerals, and principles of spectroscopy. In: Rencz, A. (Ed.), Manual of Remote Sensing. John Wiley and Sons Inc., New York. Chapter 1 in.
Clark, R.N., Roush, T.L., 1984. Reflectance spectroscopy: quantitative analysis techniques for remote sensing applications. Journal of Geophysical Research 89, 6329–6340.
Clark, R.N., King, T.V.V., Gorelick, N.S., 1987. Automatic continuum analysis of reflectance spectra. Proceedings, Third AIS workshop, 2–4 June, 1987. Jet Propulsion Laboratory, JPL Publication 87–30, Pasadena, California, pp. 138–142.
Cloutis, E.A., 1996. Hyperspectral geological remote sensing: evaluation of analytical techniques. International Journal of Remote Sensing 17, 2215–2242.
Cooper, C.C., Mustard, J.F., 1999. Effects of very fine particles on reflectance spectra of smectite and palagonitic soil. Icarus 142, 557–570.
Fall, M., Sarr, A.M., 2007. Geotechnical characterization of expansive soils and their implications in ground movements in Dakar. Bulletin of Engineering Geology and the Environment 66, 279–288.
Farmer, V.C., 1974. The layer silicates. In: Farmer, V.C. (Ed.), The infra-red spectra of minerals. Mineralogical society, London, pp. 331–364.
Farmer, V.C., Russell, J.D., 1964. The infrared spectra of layer silicates. Spectrochimica Acta 20, 1149–1173.
Fityus, S., Buzzi, O., 2009. The place of expansive clays in the framework of unsaturated soil mechanics. Applied Clay Science 43, 150–155.
Fitzpatrick, E.A., 1980. SOILS; their formation, classification and distribution. Longman Inc., London, NY. 354 p.
Frost, R.L., Locos, O.B., J., R.H., Kloprogge, T., 2001. Near-infrared and mid-infrared spectroscopic study of sepiolites and palygorskities. Vibrational Spectroscopy 27, 1–13.
Fu, Z.Y., Robles-Kelly, A., Caelli, T., Tan, R.T., 2007. On automatic absorption detection for Imaging spectroscopy: a comparative study. IEEE Transactions on Geoscience and Remote Sensing 45, 3827–3844.
Gaffey, S.J., 1986. Spectral reflectance of carbonate minerals in the visible and near infrared (0.35–2.55 microns): calcite, aragonite, and dolomite. American Mineralogist 71, 151–162.
Galan, E., 2006. Genesis of clay minerals. In: Bergaya, F., Theng, B.K.G., Lagaly, G. (Eds.), Handbook of Clay Science: Developments in Clay Science, Volume 1. Elsevier, Amsterdam.
Gillot, J.E., 1987. Clay in engineering geology. Elsevier, New York.
Goetz, A.F.H., Chabrillat, S., Lu, Z., 2001. Field reflectance spectrometry for detection of swelling clays at construction sites. Field Analytical Chemistry and Technology 5, 143–155.
Gomez, C., Lagacherie, P., Coulouma, G., 2008. Continuum removal versus PLSR method for clay and calcium carbonate content estimation from laboratory and airborne hyperspectral measurements. Geoderma 148, 141–148.
Gray, J., Murphy, B., 2002. Parent material and world soil distribution, 17th World Congress of Soil Science (WCSS) Bangkok, Thailand.
Griffiths, P.R., de Haseth, J.A., 2007. Fourier Transform Infrared Spectrometry. John Wiley and Sons Inc. 529 p.
Hecker, C., Van der Meijde, M., Van der Meer, F.D., 2010. Thermal infrared spectroscopy on feldspars — successes, limitations and their implications for remote sensing. Earth-Science Reviews 103, 60–70.
Hunt, G.R., 1977. Spectral signatures of particulate minerals in the visible and near infrared. Geophysics 42, 501–513.
I.T.T., Visual Information Solutions, 2009. ENVI Version 4.7 Boulder, Colorado, USA www.ittvis.com 2009.
Johnson, J.R., Lucey, P.G., Horton, K.A., Winter, E.M., 1998. Infrared measurements of Pristine and disturbed soils 1.Spectral contrast differences between field and laboratory data. Remote Sensing of Environment 64, 34–46.
Karathanasis, A.D., Hajek, A.F., 1985. Shrink–Swell potential of montmorillonitic soils in udic moisture regimes. Soil Science Society of America 49, 159–166.
Kariuki, P.C., Van der Meer, F.D., 2003. Issues of effectiveness in empirical methods for describing swelling soils. International Journal of Applied Earth Observation and Geoinformation 4, 231–241.
Kariuki, P.C., Van der Meer, F.D., Siderius, W., 2003. Classification of soils based on engineering indices and spectral data. International Journal of Remote Sensing 24, 2567–2574.
Kariuki, P.C., Woldai, T., Van der Meer, F.D., 2004. Effectiveness of spectroscopy in identification of swelling indicator clay minerals. International Journal of Remote Sensing 25, 455–469.
Kruse, F.A., 1991. Spectral identification (1.2–2.5 μm) and characterization of Paris basin kaolinite/smectite clays using a field spectrometer. 5th colloquium on physical measurements and signatures in remote sensing. ESA, Courchevel, France, pp. 181–184.
Kruse, F.A., Kierein-Young, K.S., Boardman, J.W., 1990. Mineral mapping at Cuprite, Nevada with a 63 channel imaging spectrometer. Photogrammetric Engineering and Remote Sensing 56, 83–92.
Ludwig, B., Nitschke, R., Terhoeven-Urselmans, T., Michel, K., Flessa, H., 2008. Use of mid-infrared spectroscopy in the diffuse-reflectance mode for the prediction of the composition of organic matter in soil and litter. Journal of Plant Nutrition and Soil Science-Zeitschrift Fur Pflanzenernahrung Und Bodenkunde 171, 384–391.
Martens, H., Naes, T., 1989. Multivariate calibration. John Wiley and Sons Inc.
Michalski, J.R., Kraft, M.D., Sharp, T.G., Williams, L.B., Christensen, P.R., 2006. Emission spectroscopy of clay minerals and evidence for poorly crystalline aluminosilicates on Mars from Thermal Emission Spectrometer data. Journal of Geophysical Research 111.

Mitchell, J.K., 1993. Fundamentals of Soil behavior. John Wiley and Sons Inc., New York.
Morin, W.J., Parry, W.T., 1971. Geotechnical properties of Ethiopian volcanic soils. Geotechnique 21, 223–232.
Mustard, J.F., Murchie, S.L., Pelkey, S.M., Ehlmann, B.L., Milliken, R.E., Grant, J.A., Bibring, J.-P., Poulet, F., Bishop, J., Dobrea, E.N., Roach, L., Seelos, F., Arvidson, R.E., Wiseman, S., Green, R., Hash, C., Humm, D., Malaret, E., McGovern, J.A., Seelos, K., Clancy, T., Clark, R., Marais, D.D., Izenberg, N., Knudson, A., Langevin, Y., Martin, T., McGuire, P., Morris, R., Robinson, M., Roush, T., Smith, M., Swayze, G., Taylor, H., Titus, T., Wolff, M., 2008. Hydrated silicate minerals on Mars observed by the Mars Reconnaissance Orbiter CRISM instrument. Nature 454, 305–309.
Petit, S., 2006. Fourier Transform Infrared Spectroscopy. In: Bergaya, F., Theng, B.K.G., Lagaly, G. (Eds.), Handbook of Clay Science. : Developments in Clay Science, Volume 1. Elsevier, Amsterdam.
Rainey, M.P., Tyler, A.N., Gilvear, D.J., Bryant, R.G., McDonald, P., 2003. Mapping intertidal estuarine sediment grain size distributions through airborne remote sensing. Remote Sensing of Environment 86, 480–490.
Roush, T.L., Singer, R.B., McCord, T.B., 1987. Reflectance Spectra of selected phyllosilicates from 0.6 to 4.6 microns. Abstracts of the Lunar and Planetary Science Conference 18.
Rowan, L.C., Goetz, A.F.H., Ashley, R.P., 1977. Discrimination of hydrothermally altered and unaltered rocks in the visible and the near infrared multispectral images. Geophysics 42, 522–535.
Rowan, L.C., Mars, J.C., Simpson, C.J., 2003. Lithologic mapping in the Mountain Pass, California area using Advanced Spaceborne Thermal Emission and Reflection Radiometer (ASTER) data. Remote Sensing of Environment 84, 350–366.
Salisbury, J.W., D'Aria, D.M., 1992. Emissivity of terrestrial materials in the 8–14 μm atmospheric window. Remote Sensing of Environment 42, 83–106.
Salisbury, J.W., D'Aria, D.M., 1994. Emissivity of terrestrial materials in the 3–5 μm atmospheric window. Remote Sensing of Environment 47, 345–361.
Salisbury, J.W., Wald, A., D'Aria, D.M., 1994. Thermal-infrared remote sensing and Kirchhoff's law 1. Laboratory measurements. Journal of Geophysical Research 99, 11,897–11,911.
Seco, A., Ramirez, F., Miqueleiz, L., Garcia, B., 2011. Stabilization of expansive soils for use in construction. Applied Clay Science 51, 348–352.
Seed, H.B., Woodward, R.J., Lundgren, R., 1962. Prediction of swelling potential for compacted clays. Journal of the Soil Mechanics and Foundation Division Proceedings of the American Society of Civil Engineers 88, 53–88.
Selige, T., Bohner, J., Schmidhalter, U., 2006. High resolution topsoil mapping using hyperspectral image and field data in multivariate regression modeling procedures. Geoderma 136, 235–244.
Shepherd, K.D., Vanlauwe, B., Gachengo, C.N., Palm, C.A., 2005. Decomposition and mineralization of organic residues predicted using near infrared spectroscopy. Plant and Soil 277, 315–333.
Shi, B., Jiang, H., Liu, Z., Fang, H.Y., 2002. Engineering geological characteristics of expansive soils in China. Engineering Geology 67, 63–71.
Skempton, A.W., 1984. The colloidal activity of clays. In: Skempton, A.W. (Ed.), Selected papers on Soil Mechanics. Thomas Telford Limited, London, p. 281.
Snethen, D.R., 1975. A Review of Engineering Experiences with Expansive Soils in Highway Subgrades. Federal Highway Administration Office of Research and Development, Washington D.C.
Sridharan, A., Gurtug, Y., 2004. Swelling behavior of compacted fine-grained soils. Engineering Geology 72, 9–18.
Sunshine, J.M., Pieters, C.M., Pratt, S.F., 1990. Deconvolution of mineral absorption-bands — an improved approach. Journal of Geophysical Research-Solid Earth and Planets 95, 6955–6966.
Thomas, P.J., Baker, J.C., Zelazny, L.W., 2000. An Expansive soil index for predicting shrink–swell potential. Soil Science Society of America 64, 268–274.
Van der Meer, F.D., 1995. Spectral Reflectance of carbonate mineral mixtures and bidirectional theory: quantitative analysis techniques for application in remote sensing. Remote Sensing Reviews 13, 69–94.
Van der Meer, 1999. Can we map swelling clay with remote sensing? International Journal of Applied Earth Observation and Geoinformation 1, 27–35.
Van der Meer, 2004. Analysis of spectral absorption features in hyperspectral imagery. International Journal of Applied Earth Observation and Geoinformation 5, 55–68.
Viscarra Rossel, R.A., Walvoort, D.J.J., McBratney, A.B., Janik, L.J., Skjemstad, J.O., 2006. Visible, near infrared, mid infrared or combined diffuse reflectance spectroscopy for simultaneous assessment of various soil properties. Geoderma 131, 59–75.
Viscarra Rossel, R.A., Cattle, S.R., Ortega, A., Fouad, Y., 2009. In situ measurements of soil colour, mineral composition and clay content by Vis-NIR spectroscopy. Geoderma 150, 253–266.
Waiser, T.H., Morgan, C.L.S., Brown, D.J., Hallmark, C.T., 2007. In situ characterization of soil clay content with visible near-infrared diffuse reflectance spectroscopy. Soil Science Society of America 71, 389–396.
Wold, S., Sjostrom, M., Eriksson, L., 2001. PLS-regression: a basic tool of chemometrics. Chemometrics and Intelligent Laboratory Systems 58, 109–130.
Yitagesu, F.A., Van der Meer, F.D., Van der Werff, H., 2009. Quantifying engineering parameters of expansive soils from their reflectance spectra. Engineering Geology 105, 151–160.
Yong, R.N., Warkentin, B.P., 1975. Soil properties and behavior. Elsevier scientific publishing company, Amsterdam, Oxford, New York.